Title
Parkfield earthquakes: Characteristic or complementary?

Journal
Journal of Geophysical Research-Solid Earth, 112

ISSN
0148-0227

Authors
Custodio, Susana
Archuleta, Ralph J.

Publication Date
2007-05-01

DOI
10.1029/2006JB004617

Peer reviewed

Parkfield Earthquakes: Characteristic or Complementary?

Susana Custódio and Ralph J. Archuleta

Institute for Crustal Studies, Department of Earth Science, University of California, Santa Barbara, California, USA

Journal of Geophysical Research

Submitted on July 7, 2006

Revised on January 15, 2007

Published on May 22, 2007

Index terms: 7200 – Seismology; 7215 - Earthquake source observations; 7223 - Earthquake interaction, forecasting, and prediction; 0545 - Modeling; 3260 – Inverse theory; 7209 – Earthquake dynamics

Susana Custódio, Institute for Crustal Studies, University of California at Santa Barbara, Girvetz Hall 1140, Santa Barbara, CA 93106, USA (susana@crustal.ucsb.edu)

Abstract

We model the two most recent ~M_w6 Parkfield, California, earthquakes, which occurred in 1966 and 2004, from a non-linear global inversion of near-fault strong-motion seismograms. Our rupture models are characterized by spatially variable slip amplitude and rake, rupture velocity, and rise time. The rupture models indicate that the two earthquakes generated slip in regions of the fault that are not identical, as earlier suggested. Given the sparse seismic dataset available for the 1966 earthquake, we conduct a series of tests to verify our results: (1) we perform synthetic tests in order to study the resolution of the 1966 seismic dataset; (2) we perform an inversion of the 2004 earthquake using a dataset equivalent to the 1966 earthquake; and (3) we model the 1966 dataset under the *a priori* assumption that it was similar to the 2004 earthquake. All of the tests, as well as independent observations, indicate that slip during the 1966 and 2004 Parkfield earthquakes occurred in different regions of the fault. This result implies that regions of a fault that are frictionally locked may remain locked even during a mainshock (moderate-size earthquake). In this scenario, large earthquakes occur when all the locked regions of a fault are ”synchronized” and ready to slip at the same time.

1. Introduction

One of the open debates in seismology concerns the existence of fault sections that break repeatedly in a characteristic manner, producing "characteristic earthquakes". At a primary level, characteristic earthquakes are defined as earthquakes that occur in the same location, rupture the same fault length, and have identical faulting mechanisms and seismic moments (*Bakun and Lindh*, 1985; *Bakun et al.*, 2005). At a secondary level, characteristic earthquakes, in addition to the previous features, nucleate at the same hypocenter and propagate in the same direction (*Bakun and McEvilly*, 1984; *Bakun and Lindh*, 1985; *Bakun et al.*, 2005). A more stringent definition of characteristic earthquakes would further require consecutive events to rupture identical patches of the fault (*Bakun et al.*, 2005). The level to which earthquakes are characteristic has important implications for earthquake prediction and assessment of seismic hazard.

The Parkfield section of the San Andreas Fault in California is a prime example of a characteristic fault section. In historical times it generated ~M_w6 right-lateral strike-slip earthquakes in 1881, 1901, 1922, 1934, 1966 and most recently in 2004 (earthquakes close to Parkfield may also have occurred in 1877 and 1908) (*Bakun and McEvilly*, 1979; *Toppozada et al.*, 2002). Data permit a common epicenter, beneath Middle Mountain (Figure 1), for the 1922, 1934 and 1966 earthquakes (*Bakun and McEvilly*, 1984). Moreover, the 1934 and 1966 earthquakes generated identical regional and teleseismic waveforms; they are thought to have ruptured unidirectionally to the southeast over the same fault length; and they were preceded by co-located M_L5.1 foreshocks that occurred 17 minutes prior to the respective mainshocks (*Bakun and McEvilly*, 1979; *Bakun and Lindh*, 1985).

The 2004 Parkfield earthquake was a surprise for the seismological community - whereas the earthquake had been anticipated for years, its character was not consistent with the predictions. Unlike previous events, the 2004 earthquake nucleated close to Gold Hill (Figure 1), which is located 20 km southeast of Middle Mountain (epicenter of earlier M_w6 events), it ruptured toward the northwest, and it was not preceded by foreshocks or any other precursors (*Bakun et al.*, 2005; *Johnston et al.*, 2006). A question that remains open is whether the slip distribution of the 2004 earthquake was similar to that of previous Parkfield M_w6 events. In other words, did the 2004 Parkfield earthquake rupture the same fault patches as previous events? The two most recent Parkfield earthquakes – 1966 and 2004 – were recorded by strong-motion seismographs located close to the fault. Using these records of ground motion we infer the time-space slip distributions of the two earthquakes and then analyze the similarities between the two earthquakes.

In order to model the 1966 and 2004 Parkfield earthquakes we apply a non-linear inversion algorithm (*Liu and Archuleta*, 2004; *Liu et al.*, 2006) to strong-motion seismograms recorded less than 20 km from the fault. The algorithm generates multiple random space-time slip distributions, which are used to forward compute synthetic ground motion. From the comparison of the synthetic ground motion with the observed ground motion, the algorithm chooses the "best" rupture model (i.e., the space-time slip distribution that leads to synthetic ground motion that most adequately resembles the observed ground motion). Because the velocity structure at Parkfield is highly heterogeneous (*Eberhart-Phillips and Michael*, 1993; *Thurber et al.*, 2003, 2006) and the site effects are very strong (*Liu et al.*, 2006), we use site amplification factors and a weighting scheme to correct the data for site amplification and local resonances.

The 2004 earthquake rupture model is based on ground motion recorded at 43 stations well distributed around the fault plane. In contrast, the 1966 earthquake model is based on data recorded at only five stations, all of them located on the southeast end of the rupture plane. In order to understand which features of the 1966 model we can be confident about, we perform three different tests. The first test makes use of synthetic rupture models. We start by generating simple rupture models, based on which we compute ground-motion. We then add white noise to the synthetic ground-motion, and try to recover the initial rupture models by inversion of the noisy synthetic dataset. The degree to which the initial models can be recovered is an indicator of the resolution of the dataset. In the second test, we compute a model for the 2004 earthquake using a dataset equivalent to the 1966 dataset. More specifically, we use data from only five stations, all located close to those that recorded the 1966 earthquake, to infer a rupture model for the 2004 earthquake. The differences between the 1966 and 2004 rupture models, as obtained from data recorded at the same stations, will highlight effective differences between the two earthquakes. In the last test, we compute a model for the 1966 earthquake while constraining the slip amplitude to be similar to the 2004 earthquake. We then analyze how well this constrained model can replicate the observed ground motion. Finally, we compare our results with independent studies.

2. Slip model for the 1966 and 2004 earthquakes

The 1966 earthquake was recorded by only five strong ground-motion seismographs (*Housner and Trifunac,* 1967), all of them located along a line perpendicular to the fault on the SE end of the rupture zone (Figure 1). The station closest to the fault – CH2W – recorded a large peak velocity of ~35 cm/s in the fault-normal direction. Unfortunately this instrument did not record the fault-parallel motion. Previous strong-motion studies of the 1966 Parkfield earthquake can be grossly divided into two groups: (1) those that postulate shallow slip and model only the fault-normal ground motion recorded at station CH2W (e.g. *Aki* (1968)); and (2) those that model slip over a wider fault plane (~ 40km x 8km, in agreement with aftershock locations) and obtain a good fit to data recorded at all stations except CH2W, where the ground motion predicted from the models is always less than what was observed (e.g. *Anderson* (1974)). Most of these earlier studies (1) model the medium around the fault as a homogeneous infinite space; (2) they assume spatially uniform slip amplitude, rake angle, rupture velocity and rise time over the fault plane and (3) they model surface displacements (*Aki*, 1968; *Haskell*, 1969; *Boore et al.*, 1971; *Trifunac and Udwadia*, 1974; *Anderson*, 1974, among others). *Trifunac and Udwadia* (1974) were the first to apply a least-squares inversion scheme to the seismic data in order to obtain slip amplitude. They divided the fault plane into seven sections, and allowed each section to have different slip amplitudes. For the whole fault they postulated uniform rupture velocity and rise time. *Archuleta and Day* (1980) presented a quasi-dynamic model for the 1966 Parkfield earthquake assuming constant rupture velocity. Previous studies using the strong-motion data were done more than 20 years ago, when methods were not as refined and computers were not as efficient as today. Our kinematic rupture model is the first resulting from a global inversion of the 1966 available seismic dataset (i.e., our model results from a search for the global minimum of the entire space of possible models). Our space-time rupture model allows spatially variable slip amplitude and rake, rupture velocity, and rise-time. Wave propagation is computed assuming a layered velocity structure that is different for each side of the fault. We fit ground velocities instead of displacements, which leads to more control on the distribution of kinematic parameters.

Because of the prediction that an earthquake would occur in Parkfield between 1983 and 1993 (*Bakun and McEvilly*, 1984), the geophysical instrumentation in Parkfield was strongly intensified in 1985 (*Bakun and Lindh*, 1985; *Roeloffs and Lagbein*, 1994; *Roeloffs*, 2000). When the earthquake finally occurred in 2004, it generated an excellent dataset useable for inversions. In particular, 56 near-fault strong-motion seismographs recorded the earthquake (*Shakal et al.*, 2005, 2006).

In a previous paper *Liu et al.* (2006) obtained a rupture model for the 2004 earthquake from inversion of the strong-motion dataset. Here, we derive a model for the 1966 earthquake following the same procedure that they used. The data processing and modeling is explained in depth in *Liu et al.* (2006), thus we will not repeat it here. Instead, we will review the most important aspects of their modeling and refer the reader to their paper for further details.

2.1. Data Processing

We model the 1966 earthquake based on ground motion recorded at five stations – CH2W, CH5W, CH8W, CH12W and TEMB (Figure 1). The 2004 earthquake is modeled from ground motion recorded at 43 stations – CH1E, CH2E, CH2W, CH3E, CH3W, CH4AW, CH4W, COAL, DFU, EFU, FFU, FZ1, FZ3, FZ4, FZ6, FZ7, FZ8, FZ9, FZ11, FZ12, FZ15, GFU, GH1W, GH2E, GH3E, GH3W, GH5W, JFU, KFU, MFU, PHOB, SC1E, SC2E, SC3E, RFU, TEMB, VC1W, VC2E, VC2W, VC3W, VC4W, VC5W, VFU. These 43 stations are chosen from the available 56 based on data quality (*Liu et al.*, 2006). The strong-motion stations record ground accelerations that we integrate to obtain ground velocity. The velocity waveforms are filtered in the passbands 0.25-1 Hz (1966 earthquake) and 0.16-1 Hz (2004 earthquake) with a 4-pole zero-phase (forward and backward) Butterworth filter. The lower limit of the passband is based on the quality of the ground motion record; the upper limit is chosen based on the quality of the velocity structure approximation we use.

We use an approximation to site effects in order to correct for amplifications and resonances (*Liu et al.*, 2006). This correction is based on data recorded by the Parkfield array during the 1983 M_w6.5 Coalinga earthquake, which occurred 25 km NE of Parkfield. The correction has two components:

1. Amplification. This correction is applied when the ground motion is amplified over all the frequency range of interest to us. Based on observations of the Coalinga earthquake, we compute the factor by which ground motion is amplified at each station due to site conditions. We then divide each observed waveform by the corresponding station amplification factor. This correction is frequency-independent.

2. Resonance. We account for frequency resonances (i.e., amplification of ground motion at particular frequencies) by using a weighting scheme; stations strongly affected by resonances are downweighted in our inversion.

For the rest of the paper we will use the word "observation" to refer to the velocity waveforms obtained through this process.

2.2. Non-Linear Global Inversion

We use the non-linear simulated annealing inversion scheme of *Liu and Archuleta* (2004) to infer a rupture model from the observed ground motion. The rupture model is defined by five source parameters: slip amplitude (amount of slip), rake angle (direction of slip), average rupture velocity (related to the time it takes for the rupture to propagate from the hypocenter to a given point on the fault) and rise time (time interval during which a point on the fault slips). The rise time is defined as the sum of two independent time parameters: the time during which slip accelerates and the time during which slip decelerates. The simulated annealing algorithm starts by generating very dissimilar random rupture models, for which synthetic ground motion is computed. By comparing synthetic and observed ground motion, the algorithm proceeds with the most adequate rupture model. In the next step, the algorithm generates random rupture models that resemble the best rupture model from the previous iteration. As the number of iterations increases, the random models become more similar to the previous best model (the amplitude of the random variations around the preferred model is decreased), allowing for fine-tuning of the rupture model. Instead of evaluating all possible rupture models, the simulated annealing algorithm relies on an adequate sampling of the parameter space. The sampled models are generated in a random way; it is thus possible to obtain multiple preferred rupture models by making the inversion follow different random paths. In other words, it is possible to arrive at different final rupture models by sampling different random rupture models as we iterate through. If the inversion algorithm works correctly, all final rupture models look alike, independently of the random path that the algorithm took to arrive at the final model.

For each different trial rupture model, synthetic ground motion is computed and compared with data. The goodness of fit between recorded and synthetic waveforms is quantified with a correlative misfit function (*Spudich and Miller*,1990; *Liu et al.*, 2006, equation 2). Synthetic ground motion is obtained by summing the slip contributions from a grid of points on the fault (167 m x 167 m). Green's functions and the five source parameters are computed on coarser grids of 0.5 km x 0.5 km and 2 km x 2 km, respectively. Green's functions are computed with the frequency-wavenumber method of *Zhu and Rivera* (2002) assuming a layered velocity structure (*Liu et al.*, 2006) based on 3D velocity models (*Thurber et al.*, 2003, 2006). The layered velocity structure is different for each side of the fault, thus accounting for material differences between the Franciscan and Salinian blocks on opposite sides of the San Andreas Fault. Both Green's functions and source parameters are interpolated to the finer grid of 167 m x 167 m, where the fault slip (as defined by the five source parameters) is convolved with Green's functions in order to obtain surface velocities.

Because little or no co-seismic surface break was observed during either mainshock (1966 (*Smith and Wyss*, 1968) and 2004 (*Rymer et al.*, 2006)), the fault planes that we model are buried 500 m below the surface. In our models, the fault strikes 140˚SE and dips 87˚SW (*Liu et al.*, 2006). For both mainshocks we model a rupture plane that is 10 km deep and 40 km long, in accordance with aftershock locations. In order to obtain a better fit between the locations of the aftershocks and the rupture area of each earthquake, we offset the 1966 rupture plane by 5 km along-strike to the southeast with respect to the 2004 plane (Figure 1). The coordinates of the 1966 and 2004 hypocenters are, respectively, 35.951˚N, 120.507˚W, 8.5 km deep and 35.8185˚N, 120.3706˚W, 8.26 km deep. These locations are very close to previously reported hypocenters (*McEvilly*, 1966; *Thurber et al.*, 2006), and they are adjusted so that both epicenters fall on the same previously chosen fault plane (which fits the microseismicity).

Following *Liu et al.* (2006) we impose smoothness constraints on the slip to avoid physically unrealistic abrupt variations in the rupture model. Constraints are also imposed on the seismic moment; otherwise the large areas of the fault that slip by small amounts and are not well resolved lead to a spuriously high seismic moment (*Liu et al.*, 2006).

2.3. Rupture Models

For both the 1966 and 2004 earthquakes, we compute 10 different preferred rupture models that are obtained by sampling different random models throughout the inversion (E-supp: 1966 mainshock – Figure fs01 and Tables ts01-ts10; 2004 mainshock – Figure fs02 and Tables ts11-ts20). All 10 rupture models are equally adequate, in the sense that they all have the ability to reproduce equally well the observed ground motion according to a goodness of fit for all data criterion. For each mainshock we show: (A) the rupture model that generates synthetic ground-motion that best fits the observations; and (B) the average, (C) the standard deviation, and (D) the coefficient of variation of the 10 preferred models. Given that all 10 preferred models are similarly good in fitting the observations, we find that the most robust slip distribution is given by their average. Despite showing a more diffuse image of slip on the fault, the average slip model (B) only retains the coherent features of the 10 preferred models. The standard deviation (C) is a measure of the variability between the 10 preferred models, and the coefficient of variation (D) indicates how variable the preferred models are with respect to the average.

Our rupture model for the 1966 earthquake (Figure 2) indicates that co-seismic slip occurred primarily at shallow depth and toward the SE end of the fault plane. In contrast, in 2004 peak slip occurred in a small region beneath Gold Hill surrounding the hypocenter, and further significant slip occurred 10-25 km NW of Gold Hill, at a depth between 2 and 10 km (Figure 3). We consider these features robust, as they appear in all 10 preferred rupture models (E-supp: Figures fs01 and fs02). As expected, the variability between the ten 1966 preferred models, as given by the standard deviation, is much larger than the variability between the 2004 preferred models. This is a reflection of the differences in the seismic datasets available to study the two mainshocks. The few stations that recorded the 1966 earthquake do not provide a good azimuthal coverage of the fault. It is thus important to understand which features of co-seismic slip the 1966 dataset can resolve.

3. Discussion of the 1966 Rupture Model

Our rupture models for the 1966 and 2004 earthquakes indicate that the two most recent Parkfield events ruptured fault patches that do not overlap but rather complement each other. However, the quality of the rupture models for the two earthquakes is very different – based on a better dataset, the 2004 model is better resolved than the 1966 model. How confident can we be that that the 1966 and 2004 slip distributions are in fact different?

3.1. Synthetic Tests

In order to understand the resolution of the 1966 dataset, we perform the following synthetic test:

1. We generate synthetic rupture models, which we will refer to as input rupture models (they will serve as input to the synthetic tests) – Figures 4A and 5A.

2. We generate ground motion at the 5 stations that recorded the 1966 earthquake, based on the input rupture models we created in Step 1. We will refer to this synthetic dataset as input dataset.

3. We add white noise (arbitrarily we choose the amplitude of the white noise to be 20% of the maximum amplitude in the synthetic waveform) to the input dataset created above; thus we simulate more realistic Earth-like conditions where data is contaminated by noise.

4. We use the non-linear inversion algorithm to infer a rupture model (output model) from the noisy input dataset created in Step 3.

5. For each input model we compute 10 output rupture models, as we do for the inversions of real data. The 10 models are equally adequate, in the sense that the ground motion generated by all models matches the input noisy synthetic records similarly well. Our final output model is the average of the 10 preferred models – Figures 4B and 5B.

The comparison between input and output test models suggests which features of the 1966 co-seismic slip we can recover given the available dataset. According to the synthetic tests, if slip occurs only in one small patch of the fault plane, then we are able to retrieve the correct slip distribution, independent of where slip occurs (Figure 4). However, if more than one patch of the fault slips during the earthquake, then slip that occurs on the NW end of the fault plane becomes almost unrecoverable (Figure 5). For this reason, we will limit our analysis to the SE portion of the fault plane. Note that these synthetic tests do not show a tendency for shallow slip in the output models.

3.2. Inversion of the 2004 Earthquake Using a Limited Dataset

The results of the synthetic tests are encouraging. However, the simple input models we used in the previous section (with geometrically simple regions of slip and uniform rake angle, rupture velocity and rise time) lack the complexity of a real earthquake rupture. Also, uncertainties in the velocity structure are left out in the synthetic tests. In order to assess the resolution of the 1966 earthquake given a real earthquake rupture and uncertainties in the inversion process (e.g., uncertainties in the Green's functions), we perform a second test where we invert the 2004 earthquake using only a limited dataset. For this purpose, we choose five stations (CH2W, CH4AW, CH6W, CH12W, TEMB) that recorded the 2004 earthquake, co-located or close to the stations that recorded the 1966 earthquake (Figure 1). Because station

CH8W, which recorded the 1966 earthquake, did not record the 2004 earthquake, we replaced it by station CH6W. In order to keep the stations in this limited dataset reasonably equidistant, we then also replaced station CH5W by station CH4AW. We do not use the fault-parallel component of ground motion recorded at station CH2W, in order to better reproduce the 1966 dataset. Station CH2W was moved to a new location (the two locations of station CH2W differ by only a few hundred meters) in the time interval between the two mainshocks (A. Shakal, personal communication, 2006); thus records of the two earthquakes at this station were not obtained under the exact same conditions. Because in 1966 geodetic measurements were not as accurate as today, the exact coordinates of station CH2W at the time are unknown. For the purpose of rupture modeling, it is reasonable to ignore the station relocation and assume that the station has always been at its present position.

Figure 6 shows the slip model obtained for the 2004 earthquake by inversion of the five stations. This rupture model is very different from the one obtained by inversion of the complete 2004 seismic dataset (Figure 3). The 2004 complete seismic dataset leads to a robust result; the slip distribution shown in Figure 3 is similar to those obtained by inversion of subsets of seismic data (*Custódio et al.*, 2005) and compares well with models obtained by other authors using independent datasets and inversion methods (*Liu et al.*, 2006). The striking differences between the two 2004 models, inferred from the complete dataset (Figure 3) and from the limited dataset (Figure 6), indicate that the 1966 dataset has a poor ability to resolve a complex space-time slip distribution.

In spite of the poor resolution of the sparse 1966 dataset, we can gain insight on the differences between the 1966 and 2004 earthquakes from the comparison of the two mainshock rupture models as obtained from the similar Cholame Valley datasets (Figure 7). In particular, it is worthwhile noticing that the ground-motion recorded at the five Cholame Valley stations confirms that the region of the fault that radiated most energy in 1966 is shallower and further to the southeast than in 2004. We emphasize that the available 1966 seismic dataset cannot discern a clear slip pattern; the rupture model for the 1966 earthquake (Figure 2) must be understood and interpreted within its limitations. Therefore, we will not pursue further statistical analysis regarding the correlation between the 1966 and the 2004 Parkfield earthquakes. Rather, we will investigate the hypothesis that these two earthquakes ruptured identical fault patches.

3.3. Constrained Inversion of the 1966 Earthquake

Do the data permit similar slip distributions for the 1966 and 2004 Parkfield earthquakes? In order to answer this question, we performed an inversion of the 1966 earthquake where we constrained the slip amplitude distribution to be within 20% of the 2004 slip amplitude, which is well resolved. In fact, it is possible to find an adequate model for the 1966 earthquake where the slip amplitude distribution resembles that of the 2004 earthquake. Figure 8 shows the comparison between data recorded during the 1966 earthquake and synthetic ground motion generated both from the constrained model (constrained by the 2004 slip amplitude distribution) and the unconstrained 1966 model. The synthetic waveforms generated by the two models are very similar to the observed ground motion at stations CH8W, CH12W and TEMB. At all stations, the velocity pulses arrive at the correct time and have the correct duration – our algorithm is able to find the correct phase for the waveforms by adjusting the time source parameters (rupture velocity and rise time). However, the large amplitude of the velocity pulses recorded at stations CH2W and CH5W – the stations closest to the fault – are fit only in our unconstrained model. The large velocity pulse recorded close to the fault during the 1966 event, which quickly attenuates with distance from the fault, requires a significant amount of shallow slip around Gold Hill. Site effects can account only for a portion of the large velocities recorded close to the fault in 1966. Indeed, we included in this study an approximation to site effects (*Liu et al.*, 2006) in order to account for amplification and frequency resonance at the different stations. Due to this amplification correction, we only try to fit a maximum peak velocity of 20 cm/s at station CH2W, whereas the recorded peak velocity at this station was 35 cm/s.

3.4. Comparison with Independent Data

Inversions of geodetic data (*Segall and Du*, 1993; *Murray and Langbein*, 2006) indicate that slip in the 1934 and 2004 Parkfield earthquakes occurred mainly on the NW Parkfield fault section, close to Middle Mountain, whereas in 1966 slip occurred predominantly to the SE, around Gold Hill. Thus the geodetic studies agree well with our results inferred from strong-motion data. Like the seismic data, the geodetic data clearly do not permit identical slip distribution for the 1966 and 2004 earthquakes (*Murray and Langbein*, 2006), and further exclude the hypothesis that the 1934 and 1966 earthquakes were identical (*Segall and Du*, 1993).

Figure 9 shows aftershocks of both the 1966 and 2004 earthquakes (*Thurber et al.*, 2006). Due to disparities in dataset quality, the 2004 aftershocks are more precisely located (double difference locations) than the 1966 aftershocks (absolute locations with respect to the assumed velocity structure). Also, the stations that recorded the 1966 aftershocks were deployed around Gold Hill, which explains the reduced number of located aftershocks to the NW of the fault section. Toward the SE, where the 1966 catalog is more complete, 1966 aftershocks extend further SE than 2004 aftershocks. Some of the 1966 aftershocks are shallow, surrounding the region of high slip in our model (Figure 9). Aftershocks of the 2004 earthquake overlap background microseismicity and 1966 aftershocks, but specially illuminate seismic spots toward the NW of the Parkfield fault section. This aftershock pattern agrees with a larger region of slip toward the NW and with the effect of stress loading due to directivity of a northwestward propagating rupture in 2004.

Teleseismic waves due to the 1922, 1934, 1966 and 2004 were recorded in De Bilt, Netherlands (*Bakun and McEvilly*, 1984; *Dost and Haak*, 2006). The seismograms of the four events are similar, as expected for earthquakes of similar sizes that occurred in the same location with a similar focal mechanism. From the four Parkfield events, the 1966 earthquake generated the most dissimilar records of the set (*Dost and Haak*, 2006), indicating first order differences between the 1966 and 2004 ruptures.

Wu (1968) studied the 1966 Parkfield earthquake from local strong-motion seismometer and seismoscope records, regional short-period seismometer records and long-period teleseismic records. He concluded that the magnitude of the 1966 earthquake as inferred from surface waves (M_S=6.5) is much larger than inferred from other measurements (M_b=5.9, M_L=5.5). The efficient excitation of surface waves supports the existence of shallow slip in 1966 that we infer from our modeling. *Aki* (1968) also inferred that in 1966 most energy was radiated from a shallow depth. He arrived at this conclusion by combining the dislocation estimated from strong-motion near-fault records with the seismic moment obtained from long-period surface waves (*Tsai and Aki*, 1969)

4. Implications for Earthquake Prediction

Our results, obtained from the analysis of seismic strong-motion data, strongly suggest that the 1966 and 2004 Parkfield earthquakes did not rupture identical regions of the Parkfield fault section. Our interpretation that at least to some extent the 1966 and 2004 ruptures complement each other is supported by geodetic studies, aftershock locations, comparison of teleseismic waveforms and surface wave observations. An identical behavior of earthquakes that rupture complementary zones of the same fault plane is observed in Papua New Guinea (*Park and Mori*, in press). *Okada et al.* (2005) studied the most recent (post 1930's) moderate and large earthquakes in Miyagi-Oki, Japan, and proposed that *"several asperities exist offshore of Miyagi Prefecture, and (...) those asperities rupture repeatedly at sometime simultaneously and other time separately"*. On a larger scale, similar patterns are observed in subduction zones (e.g., Alaska (*Sykes*, 1971), Chile (*Comte et al.*, 1986; *Campos et al.*, 2002)). Here, different fault sections rupture individually or together, complementing previous ruptures, so that eventually the entire subduction zone has slipped co-seismically.

The persistence of microseismicity in Parkfield suggests that intrinsic fault properties (e.g. rheology, geometry) control the seismicity. This observation implies the existence of asperities (regions of the fault that are strongly coupled, i.e., frictionally locked) that persist over multiple earthquake cycles. To reconcile the existence of persistent asperities with our observation of different slip distributions in consecutive Parkfield earthquakes, we propose a scenario where the fault contains different asperities, each of which has its own frictional properties and thus ruptures at a different time. Within this framework we hypothesize that if all asperities are synchronized, i.e. simultaneously loaded, then a major earthquake will happen. We can speculate that this was the case in 1857, when two Parkfield earthquakes (~M5.6 and ~M6.1) shortly preceded the great Fort Tejon earthquake by a few hours (*Sieh*, 1978b). The ~M8 Fort Tejon earthquake was the last large earthquake to rupture the south-central San Andreas Fault. It nucleated in Parkfield

(Cholame Valley) and ruptured ~400 km south until Wrightwood (*Sieh*, 1978a).

The Parkfield Experiment yielded a dataset of exceptional quality for the 2004 earthquake; we expect that the next Parkfield earthquakes will generate at least equally good datasets. Parkfield remains as a very good location to trap ~M_w6 earthquakes, and given the knowledge we already have of past Parkfield events, a thorough recording and study of future events will certainly contribute significantly to our understanding of seismicity and loading patterns. The Parkfield Experiment remains of great value to the physical understanding of earthquake interaction, and therefore to earthquake forecast.

5. Conclusions

We used strong ground-motion recorded by five near-field seismographs to infer a kinematic rupture model for the 1966 M_w6 Parkfield earthquake. Because this earthquake was recorded by a very limited number of instruments, we conducted a number of tests to assess the resolution of our rupture model. In particular, we focused on the hypothesis of similar slip distributions in the 1966 and 2004 earthquakes. We concluded that slip in the two most recent Parkfield events (1966 and 2004) did not occur in a characteristic manner, but rather occurred in a complementary way. The most robust result of our analysis is that slip in the 1966 earthquake occurred further SE than in the 2004 earthquake. In order to explain the complementary character of the 1966 and 2004 slip distributions, while taking in account the characteristic behavior of microseismicity in Parkfield, we propose the existence of several asperities along the Parkfield section of the San Andreas Fault, each of which having its own frictional properties. In this scenario, characteristic earthquakes may occur if the same asperities reach their yield stress simultaneously. If all the asperities on the fault reach their yield stress at approximately the same time, then a larger earthquake may result.

Acknowledgments.

We thank the California Geological Survey (CGS) and the United States Geological Survey (USGS) for the data used in this study. S. Custódio is the recipient of a PhD fellowship (SFRH/BD/14353/2003) from the Portuguese Foundation for Science and Technology (FCT). This work was supported by the National Science Foundation (EAR-0512000) and by the Southern California Earthquake Center. SCEC is funded by NSF Cooperative Agreement EAR-0106924 and USGS Cooperative Agreement 02HQAG0008. This is SCEC contribution number 1008 and ICS contribution number 0734.

References

Aki, K. (1968), Seismic displacements near a fault, *J. Geophys. Res.*, *73*, 5359–5376.

Anderson, J. (1974), A dislocation model for the Parkfield earthquake, *Bull. Seism. Soc. Am.*, *64*(3-1), 671–686.

Archuleta, R. J., and S. M. Day (1980), Dynamic rupture in a layered medium; the 1966 Parkfield earthquake, *Bull. Seism. Soc. Am.*, *70*(3), 671–689.

Bakun, W. H., and A. G. Lindh (1985), The Parkfield, California, earthquake prediction experiment, *Science*, *229*, 619–624.

Bakun, W. H., and T. V. McEvilly (1979), Earthquakes near Parkfield, California: Comparing the 1934 and 1966 Sequences, *Science*, *205*, 1375–1377.

Bakun, W. H., and T. V. McEvilly (1984), Recurrence models and Parkfield, California, earthquakes, *J. Geophys. Res.*, *89*(18), 3051–3058, doi: 10.1029/0JGREA0000890000B5003051000001.

Bakun, W. H., et al. (2005), Implications for prediction and hazard assessment from the 2004 Parkfield earthquake, *Nature*, *437*, 969 – 974.

Boore, D. M., K. Aki, and T. Todd (1971), A two-dimensional moving dislocation model for a strike-slip fault, *Bull. Seism. Soc. Am.*, *61*(1), 177–194.

Campos, J., et al. (2002), A seismological study of the 1835 seismic gap in south-central Chile , *Phys. Earth Plan. Int.*, *132*, 177–195 (19).

Comte, D., A. Eisenberg, E. Lorca, M. Pardo, L. Ponce, R. Saragoni, S. K. Singh, and G. Suarez (1986), The 1985 Central Chile Earthquake: A Repeat of Previous Great Earthquakes in the Region? , *Science*, *233*, 449–453.

Custódio, S., P. Liu, and R. J. Archuleta (2005), The 2004 M_w6.0 Parkfield, California, earthquake: Inversion of near-source ground motion using multiple data sets, *Geophys. Res. Let.*, *32*, L23,312, doi: 10.1029/2005GL024417.

Dost, B., and H. W. Haak (2006), Comparing Waveforms by Digitization and Simulation of Waveforms for Four Parkfield Earthquakes Observed in Station DBN, The Netherlands, *Bull. Seism. Soc. Am.*, *96*(4B), S50–55, doi: 10.1785/0120050813.

Eberhart-Phillips, D., and A. J. Michael (1993), Three-dimensional velocity structure, seismicity, and fault structure in the Parkfield Region, central California, *J. Geophys. Res.*, *98*, 15,737–15,758.

Haskell, N. A. (1969), Elastic displacements in the near-field of a propagating fault, *Bull. Seism. Soc. Am.*, *59*(2), 865–908.

Housner, G. W., and M. D. Trifunac (1967), Analysis of accelerograms; Parkfield earthquake, *Bull. Seism. Soc. Am.*, *57*(6), 1193–1220.

Johnston, M. J. S., R. D. Borcherdt, A. T. Linde, and M. T. Gladwin (2006), Continuous borehole strain and pore pressure in the near field of the 28 September 2004 Mw 6.0 Parkfield, California, earthquake: implications for nucleation, fault response, earthquake prediction, and tremor, *Bull. Seism. Soc. Am.*, *96*(4B), S56–72, doi:

10.1785/0120050822.

Liu, P., and R. J. Archuleta (2004), A new nonlinear finite fault inversion with three-dimensional Green's functions: Application to the 1989 Loma Prieta, California, earthquake, *J. Geophys. Res.*, doi: 10.1029/2003JB002625.

Liu, P., S. Custódio, and R. J. Archuleta (2006), Kinematic inversion of the 2004 M_w6.0 Parkfield earthquake including an approximation to site effects, *Bull. Seism. Soc. Am.*, *96*(4B), S143–158, doi: 10.1785/0120050826.

McEvilly, T. V. (1966), The earthquake sequence of November 1964 near Corralitos, California, *Bull. Seism. Soc. Am.*, *56*(3), 755–773.

Murray, J., and J. Langbein (2006), Slip on the San Andreas Fault at Parkfield, California, over two earthquake cycles and the implications for seismic hazard, *Bull. Seism. Soc. Am.*, *96*(4B), S283–303, doi: 10.1785/0120050820.

Okada, T., T. Yaginuma, N. Umino, T. Kono, T. Matsuzawa, S. Kita, and A. Hasegawa (2005), The 2005 M7.2 MIYAGI-OKI earthquake, NE Japan: Possible rerupturing of one of asperities that caused the previous M7.4 earthquake, *Geophys. Res. Let.*, *32*, L24,302, doi: 10.1029/2005GL024613.

Park, S.-C., and J. Mori (in press), Are asperity patterns persistent? Implications from large earthquakes in Papua New Guinea, *J. Geophys. Res.*

Roeloffs, E. (2000), The Parkfield, California earthquake experiment: an update in 2000., *Current Science*, *79 No.9*, 1226–1236.

Roeloffs, E., and J. Langbein (1994), The earthquake prediction experiment at Parkfield, California, *Reviews of Geophysics*, *32*, 315–336.

Rymer, M. J., et al. (2006), Surface fault slip associated with the 2004 Parkfield, California, earthquake, *Bull. Seism. Soc. Am.*, *96*(4B), S11–27, doi: 10.1785/0120050830.

Segall, P., and Y. Du (1993), How similar were the 1934 and 1966 Parkfield earthquakes? , *J. Geophys. Res.*, *98*, 4527–4538.

Shakal, A., V. Graizer, M. Huang, R. Borcherdt, H. Haddadi, K. Lin, C. Stephens, and P. Roffers (2005), Preliminary analysis of strong-motion recordings from the 28 September 2004 Parkfield, California earthquake, *Seism. Res. Let.*, *76*, 27 – 39.

Shakal, A., H. Haddadi, V. Graizer, K. Lin, and M. Huang (2006), Some Key Features of the Strong-Motion Data from the M 6.0 Parkfield, California, Earthquake of 28 September 2004, *Bull. Seism. Soc. Am.*, *96*(4B), S90–118, doi: 10.1785/0120050817.

Sieh, K. E. (1978a), Slip along the San Andreas fault associated with the great 1857 earthquake, *Bull. Seism. Soc. Am.*, *68*(5), 1421–1448.

Sieh, K. E. (1978b), Central California foreshocks of the great 1857 earthquake, *Bull. Seism. Soc. Am.*, *68*(6), 1731–1749.

Smith, S. W., and M. Wyss (1968), Displacement on the San Andreas fault subsequent to the 1966 Parkfield earthquake, *Bull. Seism. Soc. Am.*, *58*(6), 1955–1973.

Spudich, P., and D. P. Miller (1990), Seismic site effects and the spatial interpolation of earthquake seismograms; results using aftershocks of the 1986 North Palm Springs, California, earthquake, *Bull. Seism. Soc. Am.*, *80*(6), 1504–1532.

Sykes, L. R. (1971), Aftershock zones of great earthquakes, seismicity gaps, and earthquake prediction for Alaska and the Aleutians, *J. Geophys. Res.*, *76 (32)*, 8021–8041.

Thurber, C., S. Roecker, K. Roberts, M. Gold, L. Powell, and K. Rittger (2003), Earthquake locations and three-dimensional fault zone structure along the creeping section of the San Andreas fault near Parkfield, CA: Preparing for SAFOD, *Geophys. Res. Let.*, *30*, 12–1, doi: 10.1029/2002GL016004.

Thurber, C., H. Zhang, F. Waldhauser, J. Hardebeck, A. Michael, and D. Eberhart-Phillips (2006), Three-dimensional compressional wavespeed model, earthquake relocations, and focal mechanisms for the Parkfield, California, region, *Bull. Seism. Soc. Am.*, *96*(4B), S38–49, doi: 10.1785/0120050825.

Toppozada, T. R., D. M. Branum, M. S. Reichle, and C. L. Hallstrom (2002), San Andreas Fault Zone, California: M□5.5 Earthquake History, *Bull. Seism. Soc. Am.*, *92*(7), 2555–2601, doi: 10.1785/0120000614.

Trifunac, M. D., and F. E. Udwadia (1974), Parkfield, California, earthquake of June 27, 1966; a three-dimensional moving dislocation, *Bull. Seism. Soc. Am.*, *64*(3), 511–533.

Tsai, Y.-B., and K. Aki (1969), Simultaneous determination of the seismic moment and attenuation of seismic surface waves, *Bull. Seism. Soc. Am.*, *59*(1), 275–287.

Wu, F. T. (1968), Parkfield earthquake of June 28, 1966: Magnitude and source mechanism, *Bull. Seism. Soc. Am.*, *58*(2), 689–709.

Zhu, L., and L. A. Rivera (2002), A note on the dynamic and static displacements from a point source in multilayered media, *Geophys. J. Int.*, *148*, 619–627, doi: 10.1046/j.1365-246X.2002.01610.x.

Figure 1. Map of the Parkfield segment of the San Andreas Fault showing the 1922, 1934 and 1966 epicenters (red star), the 2004 epicenter (blue star), aftershocks of the 1966 earthquake (red dots) (*Thurber et al.*, 2006) and aftershocks of the 2004 earthquake (blue dots) (*Thurber et al.*, 2006). The arrows show the direction of rupture – the red arrow indicates that the 1922, 1934 and 1966 earthquakes ruptured toward the SE, whereas the 2004 earthquake ruptured toward the NW (blue arrow). The fault planes modeled for the 1966 and 2004 earthquakes correspond to the red and blue lines, respectively. Note a 5 km offset between the two modeled fault planes. This offset allows a better fit of the fault planes to the aftershock locations. The seismic stations used in the study of the 1966 and 2004 earthquakes are represented by red triangles and blue inverted triangles, respectively. The gray circles indicate the five stations in the SE end of the rupture plane used to model the 2004 earthquake with a subset of data equivalent to the 1966 data set. MM - Middle Mountain; GH - Gold Hill; CH - Cholame.

Figure 2. Rupture model for the 1966 Parkfield earthquake – slip amplitude (color scale) and rupture time (white lines are 1-sec contours). Because no surface break occurred during either earthquake (1966 and 2004), the fault plane is buried 500 m below the surface. The red star marks the 1966 hypocenter. A) Best model (model that best fits the data); B) Average of 10 best models; C) Standard deviation of 10 best slip models; D) Coefficient of variation (standard deviation/average) of 10 best slip models. The average model shows only the most robust features of the 10 best models. The standard deviation indicates the variability in the rupture model. The coefficient of variation tells how variable the model is with respect to the average. MM - Middle Mountain; GH - Gold Hill; CH - Cholame.

Figure 3. Rupture model for the 2004 Parkfield earthquake – slip amplitude (color scale) and rupture time (white lines are 1-sec contours). The blue star marks the 2004 hypocenter. A) Best

model (model that best fits the data); B) Average of 10 best models; C) Standard deviation of 10 best slip models; D) Coefficient of variation (standard deviation/average) of 10 best slip models. The average model shows only the most robust features of the 10 best models. The standard deviation indicates the variability in the rupture model. The coefficient of variation tells how variable the model is with respect to the average. MM - Middle Mountain; GH - Gold Hill.

Figure 4. Synthetic tests with only one patch of slip on the fault plane. For each rupture model we show the slip amplitude (color scale) and the rupture time (white lines are 1-sec contours). A) Input rupture models. B) Output rupture models (average of 10 best models for a given synthetic dataset). The white asterisk marks the hypocenter.

Figure 5. Synthetic tests with more than one patch of slip on the fault plane. For each rupture model we show the slip amplitude (color scale) and the rupture time (white lines are 1-sec contours). A) Input rupture models. B) Output rupture models (average of 10 best models). The white asterisk marks the hypocenter. When slip occurs in more than one region of the fault, it becomes difficult to recover slip that takes place on the NW end of the fault. Also, the depth resolution deteriorates with respect to the first test case (only one region of slip on the fault). These tests do not show a tendency for shallow slip in the output models.

Figure 6. Rupture model for the 2004 Parkfield earthquake obtained from inversion of only five stations, all of them located close to the stations that recorded the 1966 earthquake. The color scale shows slip amplitude and white lines represent rupture time in 1-second contours. The blue star marks the 2004 hypocenter. A) Best model (model that best fits the data); B) Average of 10 best models; C) Standard deviation of 10 best slip models; D) Coefficient of variation (standard deviation/average) of 10 best slip models. The average model shows only the most robust features

of the 10 best models. The standard deviation indicates the variability in the rupture model. The coefficient of variation tells how variable the model is with respect to the average. MM - Middle Mountain; GH - Gold Hill.

Figure 7. Regions of largest slip in the 1966 (red) and 2004 (blue) earthquakes, as inferred from modeling of five stations in the SE end of the rupture plane. The red and blue stars mark the 1966 and 2004 hypocenters, respectively. The light and dark shaded regions correspond to parts of the fault with more than 0.3 m and 0.5 m, respectively, of co-seismic slip in our models. MM - Middle Mountain; GH - Gold Hill; CH - Cholame.

Figure 8. Comparison of two models for the 1966 earthquake: unconstrained and constrained (the slip amplitude distribution is constrained to be within 20% of the 2004 earthquake). Top: Slip amplitude distribution (color scale) and rupture time (white lines are 1-sec contours). Each model shown here is the average of the 10 best models. The red stars mark the 1966 hypocenter. The two fault planes are offset by 5 km along strike so that the 1966 constrained model can mimic the 2004 model. Bottom: Comparison between observed ground motion (black) and synthetic ground motion corresponding to each model (red). Each row shows waveforms from one station (name indicated on the left-hand side); the two horizontal components of motion (65° and 155°) are shown for each station. Vertical waveforms (not shown here) don't contain much information on the rupture (strike-slip earthquake) and were therefore strongly downweighted in the inversion. The numbers in the beginning of each waveform in the 3rd and 4th column indicate the peak velocity (cm/s) of the observed ground motion after correcting for local amplification.

Figure 9. Comparison between the rupture models for the 1966 and 2004 Parkfield earthquakes and microseismicity. A) Slip amplitude and aftershocks of the 1966 earthquake. B) Slip amplitude

and aftershocks of the 2004 earthquake. C) Aftershocks of the 1966 earthquake (red crosses), aftershocks of the 2004 earthquake (blue circles) and background seismicity from 1984 to the 2004 earthquake (gray circles) (*Thurber et al.*, in press). The size of the aftershocks (circles) is computed assuming a 3 MPa stress drop in a circular region. In the absence of information on the magnitudes of the 1966 aftershocks, we cannot compute their size; these aftershocks are represented by crosses. The rectangle indicates the position of the fault plane modeled for the 2004 earthquake. The red and blue stars mark the 1966 and 2004 hypocenters, respectively. MM - Middle Mountain; GH - Gold Hill; CH - Cholame.

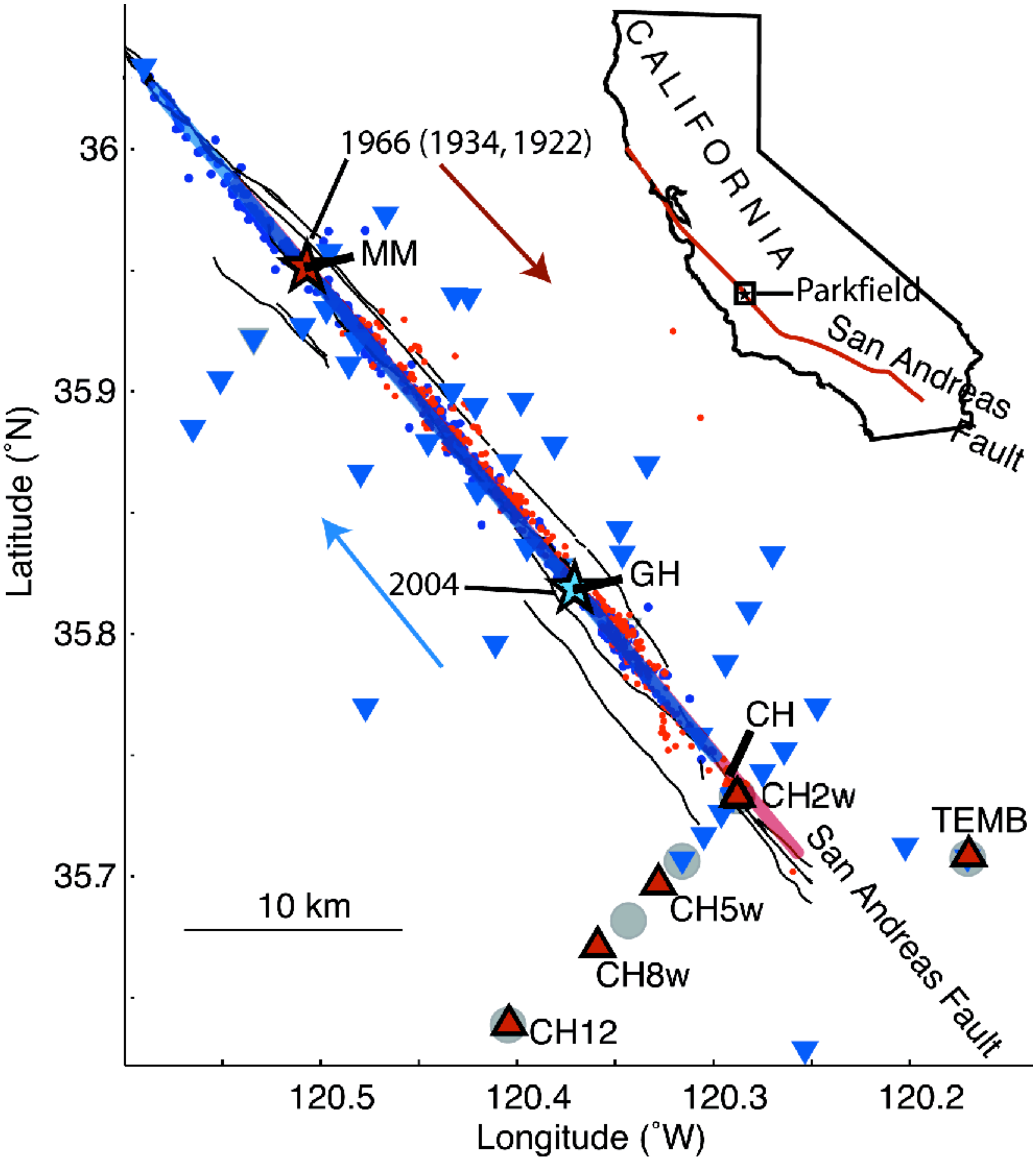

Figure 1. (1-column) Map of the Parkfield segment of the San Andreas Fault showing the 1922, 1934 and 1966 epicenters (red star), the 2004 epicenter (blue star), aftershocks of the 1966 earthquake (red dots) and aftershocks of the 2004 earthquake (blue dots). The arrows show the

direction of rupture – the red arrow indicates that the 1922, 1934 and 1966 earthquakes ruptured toward the SE, whereas the 2004 earthquake ruptured toward the NW (blue arrow). The fault planes modeled for the 1966 and 2004 earthquakes correspond to the red and blue lines, respectively. Note a 5 km offset between the two modeled fault planes. This offset allows a better fit of the fault planes to the aftershock locations. The seismic stations used in the study of the 1966 and 2004 earthquakes are represented by red triangles and blue inverted triangles, respectively. The gray circles indicate the five stations in the SE end of the rupture plane used to model the 2004 earthquake with a subset of data equivalent to the 1966 data set. MM - Middle Mountain; GH - Gold Hill; CH - Cholame.

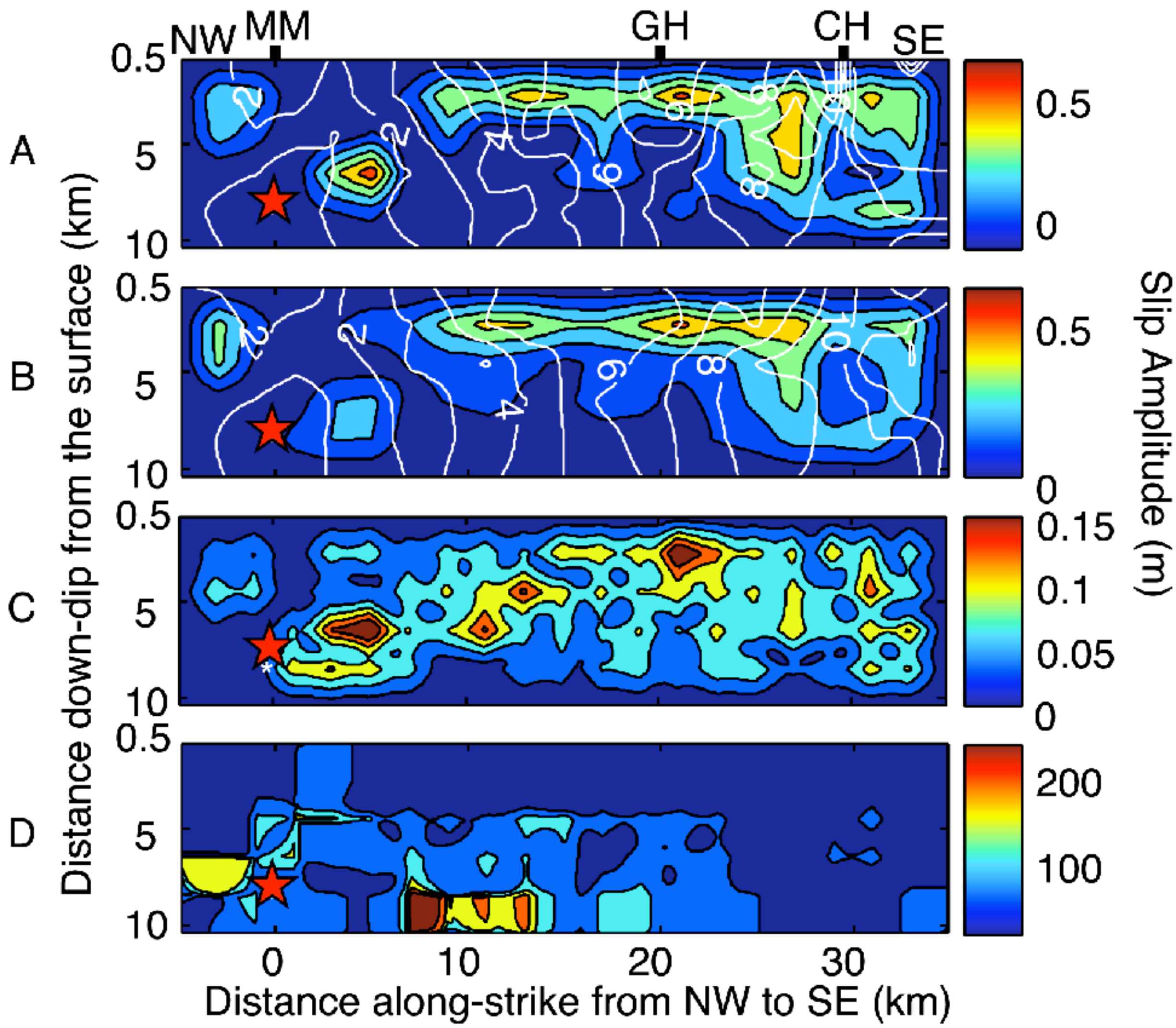

Figure 2. (1-column) Rupture model for the 1966 Parkfield earthquake – slip amplitude (color scale) and rupture time (white lines are 1-sec contours). Because no surface break occurred during either earthquake (1966 and 2004), the fault plane is buried 500 m below the surface. The red star marks the 1966 hypocenter. A) Best model (model that best fits the data); B) Average of 10 best models; C) Standard deviation of 10 best slip models; D) Coefficient of variation (standard deviation/average) of 10 best slip models. The average model shows only the most robust features of the 10 best models. The standard deviation indicates the variability in the rupture model. The coefficient of variation tells how variable the model is with respect to the average. MM - Middle

Mountain; GH - Gold Hill; CH - Cholame.

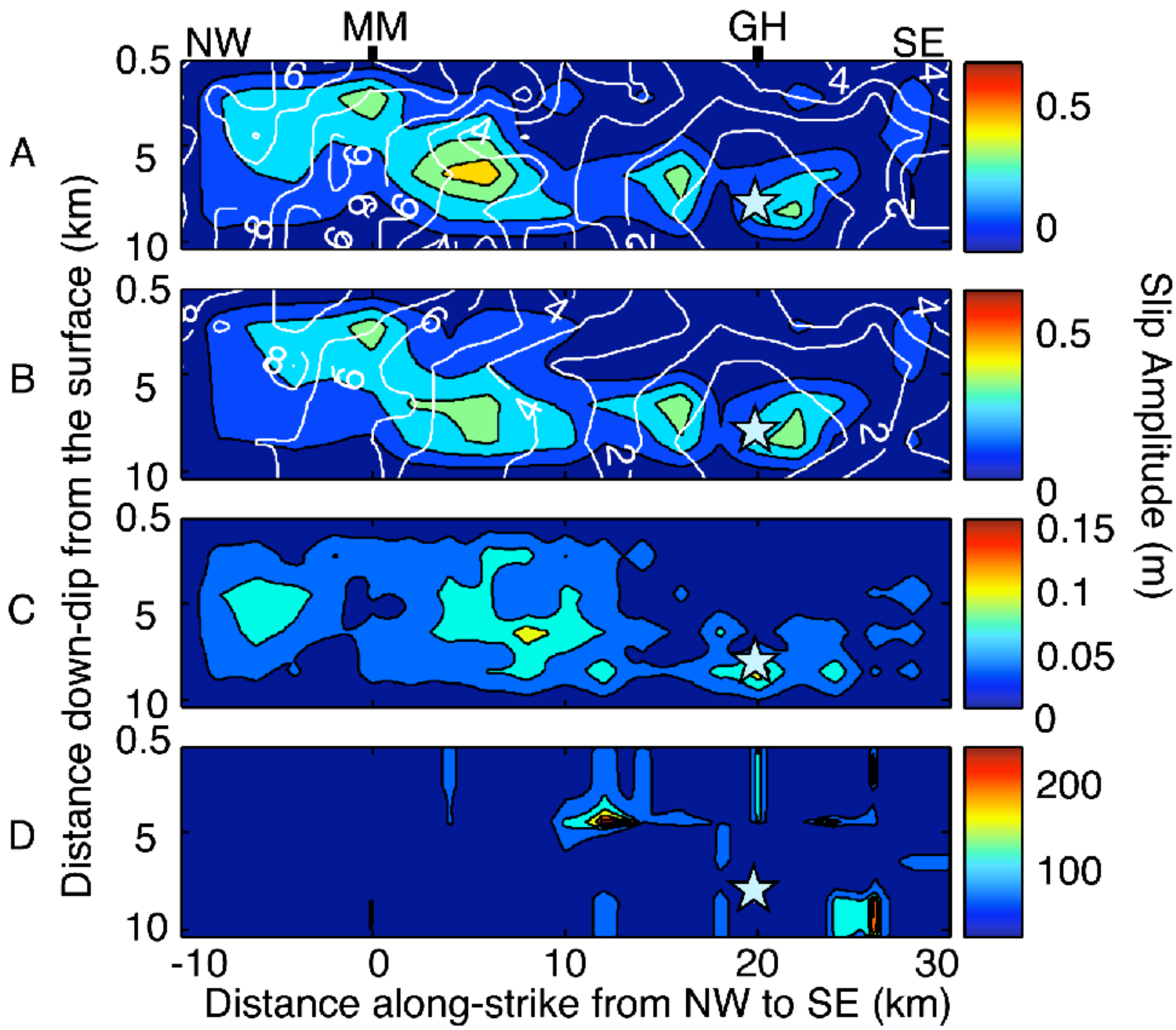

Figure 3. (1-column) Rupture model for the 2004 Parkfield earthquake – slip amplitude (color scale) and rupture time (white lines are 1-sec contours). The blue star marks the 2004 hypocenter. A) Best model (model that best fits the data); B) Average of 10 best models; C) Standard deviation of 10 best slip models; D) Coefficient of variation (standard deviation/average) of 10 best slip models. The average model shows only the most robust features of the 10 best models. The standard deviation indicates the variability in the rupture model. The coefficient of variation tells how variable the model is with respect to the average. MM - Middle Mountain; GH - Gold Hill.

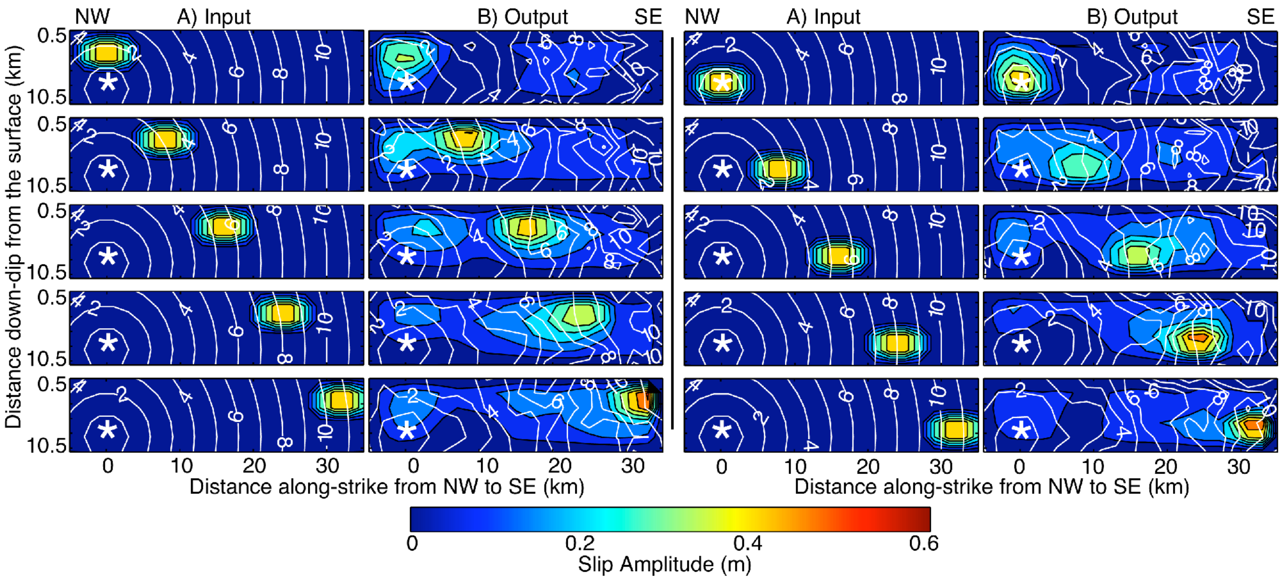

Figure 4. (2-column) Synthetic tests with only one patch of slip on the fault plane. For each rupture model we show the slip amplitude (color scale) and the rupture time (white lines are 1-sec contours). A) Input rupture models. B) Output rupture models (average of 10 best models for a given synthetic dataset). The white asterisk marks the hypocenter.

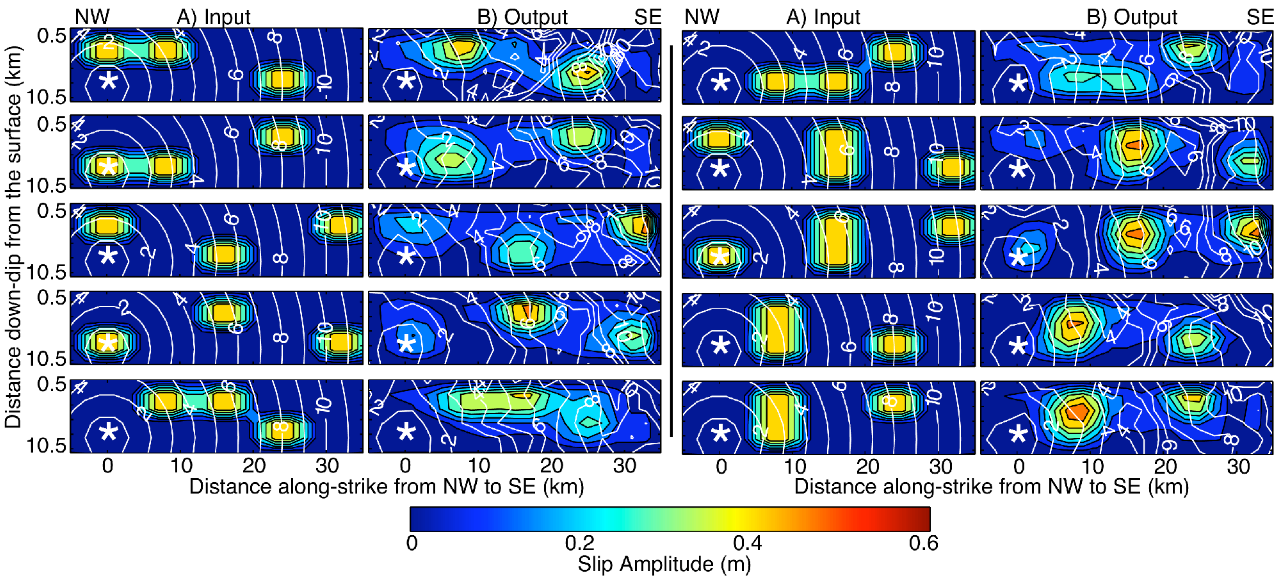

Figure 5. (2-column) Synthetic tests with more than one patch of slip on the fault plane. For each rupture model we show the slip amplitude (color scale) and the rupture time (white lines are 1-sec contours). A) Input rupture models. B) Output rupture models (average of 10 best models). The white asterisk marks the hypocenter. When slip occurs in more than one region of the fault, it becomes difficult to recover slip that takes place on the NW end of the fault. Also, the depth resolution deteriorates with respect to the first test case (only one region of slip on the fault). These tests do not show a tendency for shallow slip in the output models.

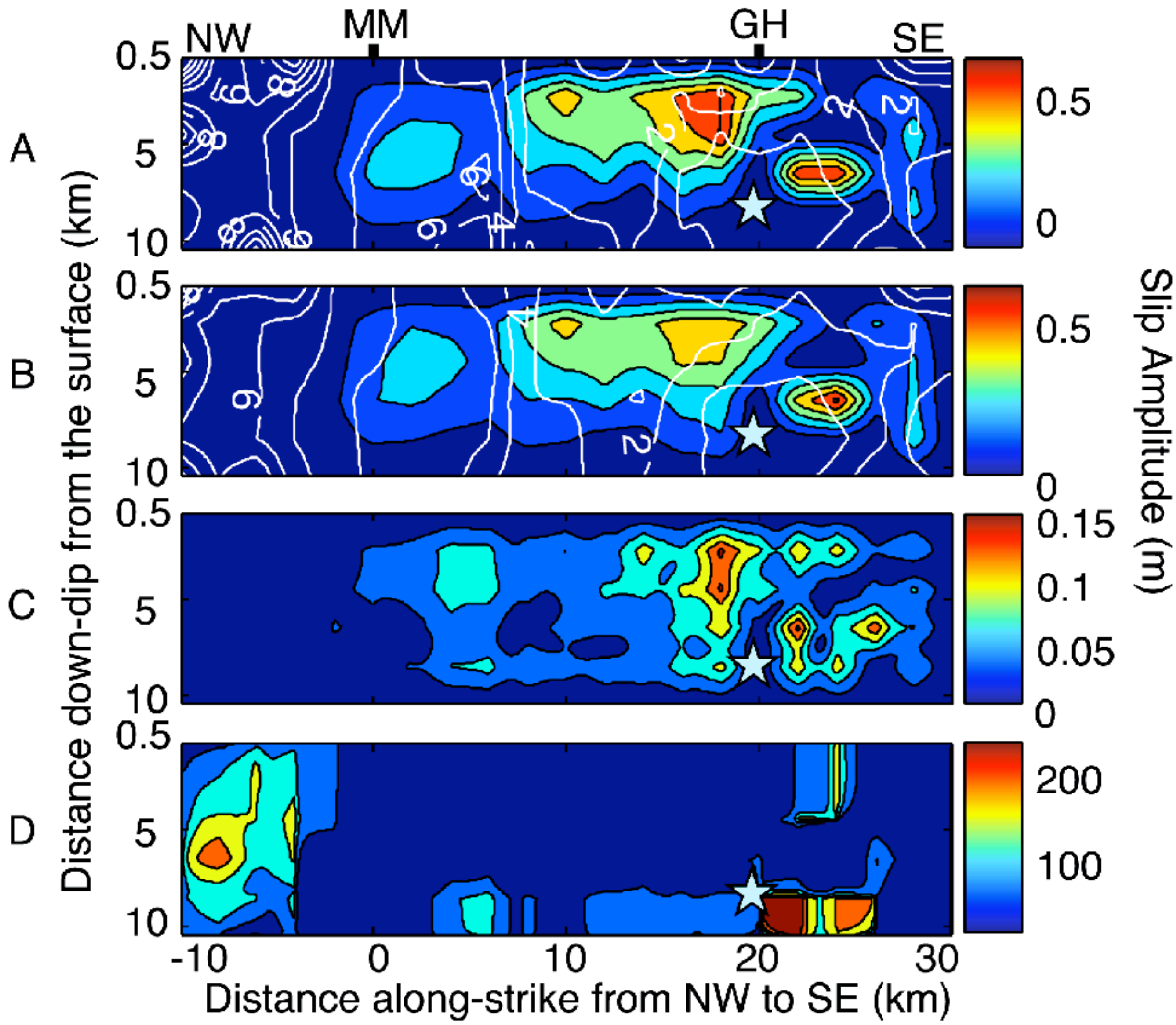

Figure 6. (1-column) Rupture model for the 2004 Parkfield earthquake obtained from inversion of only five stations, all of them located close to the stations that recorded the 1966 earthquake. The color scale shows slip amplitude and white lines represent rupture time in 1-second contours. The blue star marks the 2004 hypocenter. A) Best model (model that best fits the data); B) Average of 10 best models; C) Standard deviation of 10 best slip models; D) Coefficient of variation (standard deviation/average) of 10 best slip models. The average model shows only the most robust features of the 10 best models. The standard deviation indicates the variability in the rupture model. The coefficient of variation tells how variable the model is with respect to the

average. MM - Middle Mountain; GH - Gold Hill.

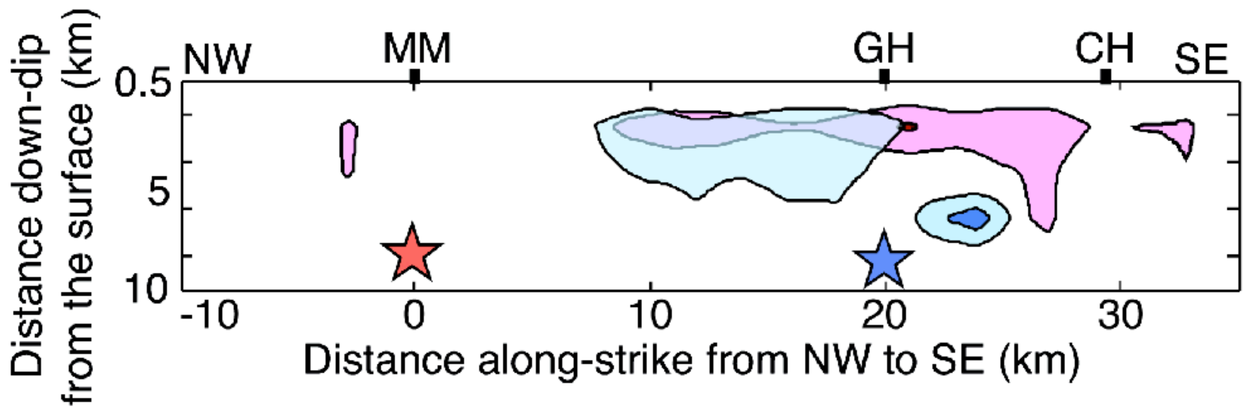

Figure 7. (1-column) Regions of largest slip in the 1966 (red) and 2004 (blue) earthquakes, as inferred from modeling of five stations in the SE end of the rupture plane. The red and blue stars mark the 1966 and 2004 hypocenters, respectively. The light and dark shaded regions correspond to parts of the fault with more than 0.3 m and 0.5 m, respectively, of co-seismic slip in our models. MM - Middle Mountain; GH - Gold Hill; CH - Cholame.

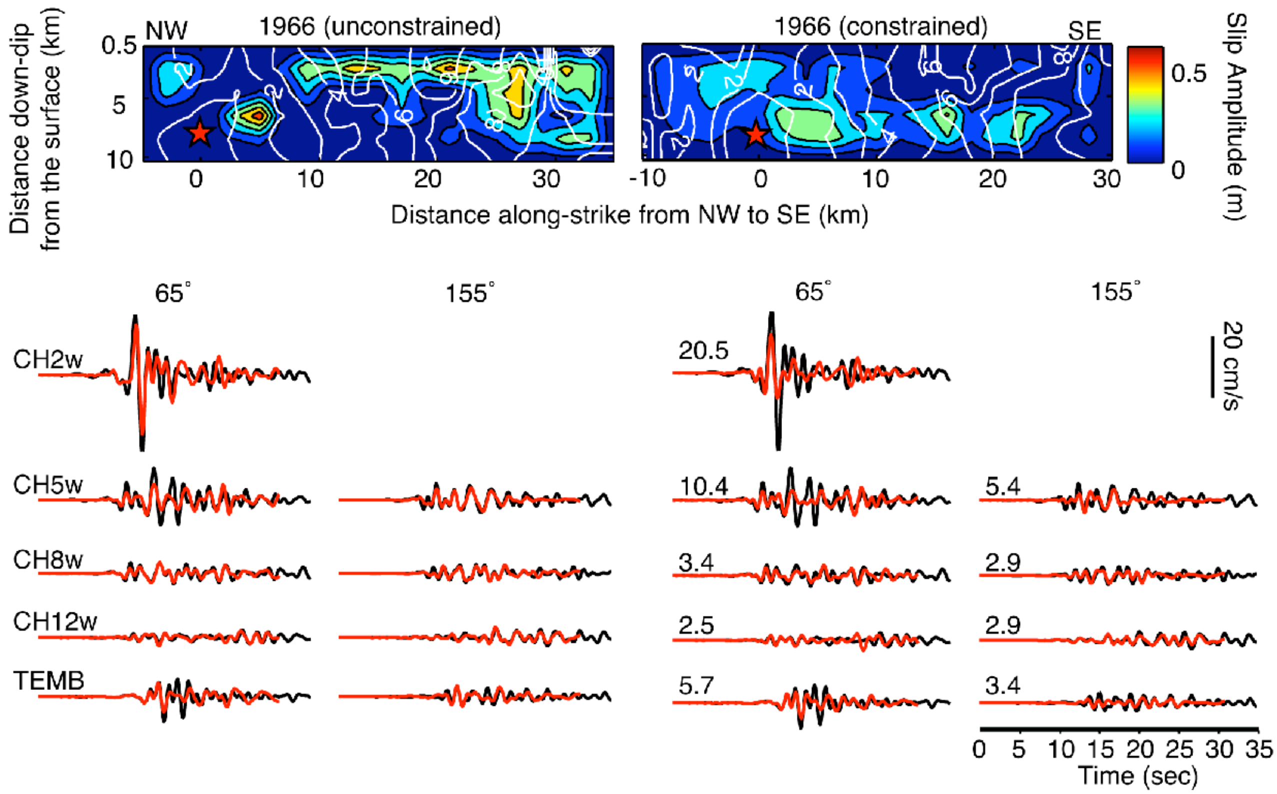

Figure 8. (2-column) Comparison of two models for the 1966 earthquake: unconstrained and constrained (the slip amplitude distribution is constrained to be within 20% of the 2004 earthquake). Top: Slip amplitude distribution (color scale) and rupture time (white lines are 1-sec contours). Each model shown here is the average of the 10 best models. The red stars mark the 1966 hypocenter. The two fault planes are offset by 5 km along strike so that the 1966 constrained model can mimic the 2004 model. Bottom: Comparison between observed ground motion (black) and synthetic ground motion corresponding to each model (red). Each row shows waveforms from one station (name indicated on the left-hand side); the two horizontal components of motion (65˚ and 155˚) are shown for each station. Vertical waveforms (not shown here) don't contain much information on the rupture (strike-slip earthquake) and were therefore strongly downweighted in the inversion. The numbers in the beginning of each waveform in the 3rd and 4th column indicate the peak velocity (cm/s) of the observed ground motion after correcting for local

amplification.

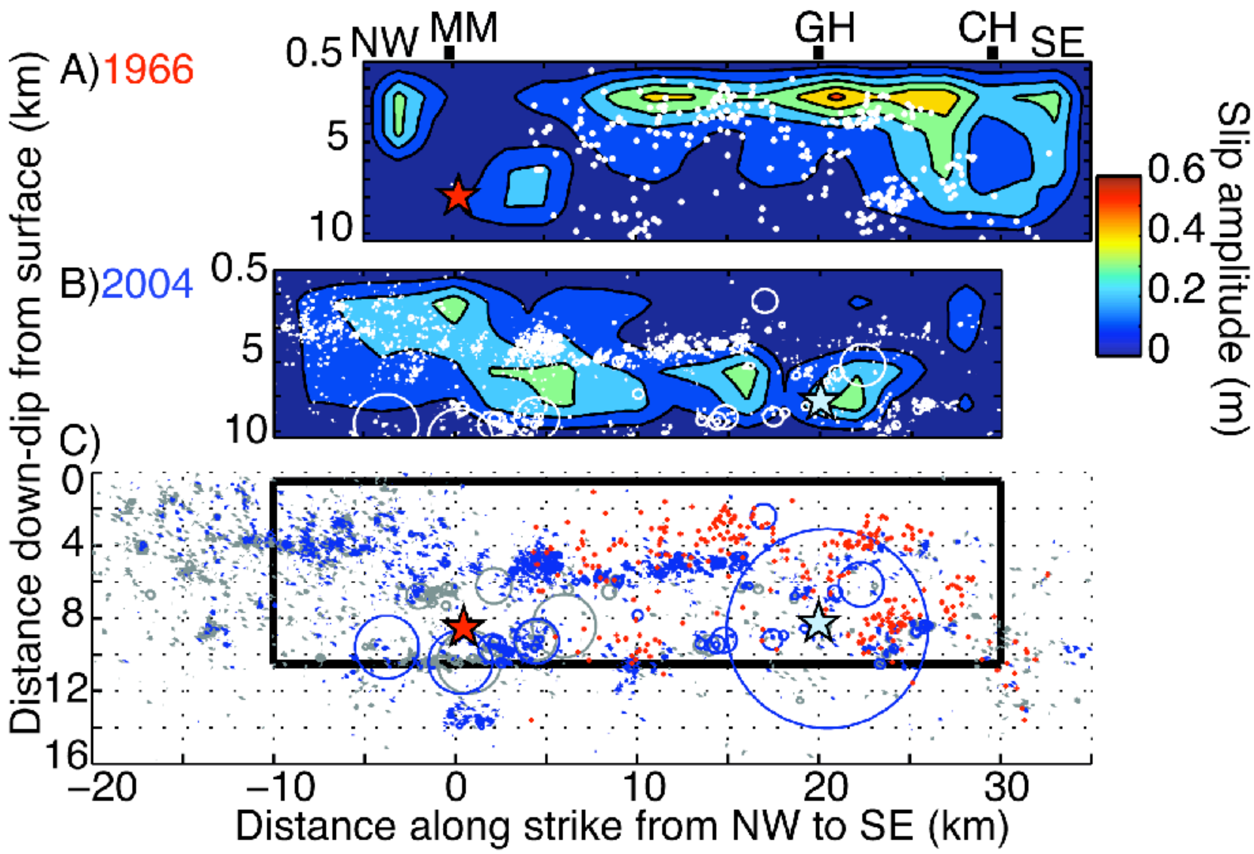

Figure 9. (1-column) Comparison between the rupture models for the 1966 and 2004 Parkfield earthquakes and microseismicity. A) Slip amplitude and aftershocks of the 1966 earthquake. B) Slip amplitude and aftershocks of the 2004 earthquake. C) Aftershocks of the 1966 earthquake (red crosses), aftershocks of the 2004 earthquake (blue circles) and background seismicity from 1984 to the 2004 earthquake (gray circles) (*Thurber et al.*, in press). The size of the aftershocks (circles) is computed assuming a 3 MPa stress drop in a circular region. In the absence of information on the magnitudes of the 1966 aftershocks, we cannot compute their size; these aftershocks are represented by crosses. The rectangle indicates the position of the fault plane modeled for the 2004 earthquake. The red and blue stars mark the 1966 and 2004 hypocenters, respectively. MM - Middle Mountain; GH - Gold Hill; CH - Cholame.

Auxiliary Material Submission for Paper 2003JBXXXXXX

Parkfield Earthquakes: Characteristic or Complementary

(Institute for Crustal Studies, University of California, Santa Barbara)

J. Geophys. Res., 108 (B6), doi:10.1029/2003JBXXXXXX, 2003

Introduction

This electronic supplement contains the complete sets of preferred rupture models that we obtained by inversion of strong-motion data, both for the 1966 and 2004 Parkfield earthquakes. The 10 preferred rupture models for the 1966 earthquake are given in tables ts01.txt through ts20.txt, and plotted in figure fs01.tif. The 2004 rupture models are given in tables ts21.txt through ts40.txt, and plotted in figure fs02.tif. Tables ts01.txt-ts10.txt and ts21.txt-ts30.txt contain the rupture models at the grid spacing at which we invert for source parameters (2km x 2km). Tables ts11.txt-ts20.txt and ts31.txt-ts40.txt contain the rupture models at the grid spacing at which we convolve the source parameters with Green's functions in order to compute synthetic ground motion (167m x 167m).

1. fs01.tif (Figure S1) Ten preferred rupture models for the 1966 Parkfield earthquake. The color scale indicates slip amplitude (m), and the white lines show 1-sec rupture time contours. The m-value above each model indicates the numerical misfit between observed ground motion and synthetic ground motion generated by each rupture model. All models are equally adequate, in the sense that they produce very similar misfits.

2. ts01.txt-ts10.txt Ten preferred rupture models for the 1966 Parkfield earthquake, given at a grid spacing of 2km x 2km (grid spacing at which we invert for source parameters). 2.1 Column "x", km, position of the grid node along-strike from NW to SE from the NW end of the fault plane. 2.2 Column "y", km, position of the grid node down-dip from the surface. 2.3 Column "amp", m, slip amplitude. 2.4 Column "rake", degrees, slip rake. 2.5 Column "rup_vel", km/s, average rupture velocity. 2.6 Column "rise1", sec, rise time during which slip accelerates. 2.7 Column "rise2", sec, rise time during which slip decelerates.

3. ts11.txt-ts20.txt Ten preferred rupture models for the 1966 Parkfield earthquake, given at a grid spacing of 167m x 167m (grid spacing at which source parameters are convolved with Green's functions in order to generate synthetic ground motion). 2.1 Column "x", km, position of the grid node along-strike from NW to SE from the NW end of the fault plane. 2.2 Column "y", km,

position of the grid node down-dip from the surface. 2.3 Column "amp", m, slip amplitude. 2.4 Column "rake", degrees, slip rake. 2.5 Column "rup_vel", km/s, average rupture velocity. 2.6 Column "rise1", sec, rise time during which slip accelerates. 2.7 Column "rise2", sec, rise time during which slip decelerates.

4. fs02.tif (Figure S2) Ten preferred rupture models for the 2004 Parkfield earthquake. The color scale indicates slip amplitude (m), and the white lines show 1-sec rupture time contours. The m-value above each model indicates the numerical misfit between observed ground motion and synthetic ground motion generated by each rupture model. All models are equally adequate, in the sense that they produce very similar misfits.

5. ts21.txt-ts30.txt Ten preferred rupture models for the 2004 Parkfield earthquake, given at a grid spacing of 2km x 2km (grid spacing at which we invert for source parameters). 2.1 Column "x", km, position of the grid node along-strike from NW to SE from the NW end of the fault plane. 2.2 Column "y", km, position of the grid node down-dip from the surface. 2.3 Column "amp", m, slip amplitude. 2.4 Column "rake", degrees, slip rake. 2.5 Column "rup_vel", km/s, average rupture velocity. 2.6 Column "rise1", sec, rise time during which slip accelerates. 2.7 Column "rise2", sec, rise time during which slip decelerates.

6. ts31.txt-ts40.txt Ten preferred rupture models for the 2004 Parkfield earthquake, given at a grid spacing of 167m x 167m (grid spacing at which source parameters are convolved with Green's functions in order to generate synthetic ground motion). 2.1 Column "x", km, position of the grid node along-strike from NW to SE from the NW end of the fault plane. 2.2 Column "y", km, position of the grid node down-dip from the surface. 2.3 Column "amp", m, slip amplitude. 2.4 Column "rake", degrees, slip rake. 2.5 Column "rup_vel", km/s, average rupture velocity. 2.6 Column "rise1", sec, rise time during which slip accelerates. 2.7 Column "rise2", sec, rise time during which slip decelerates.

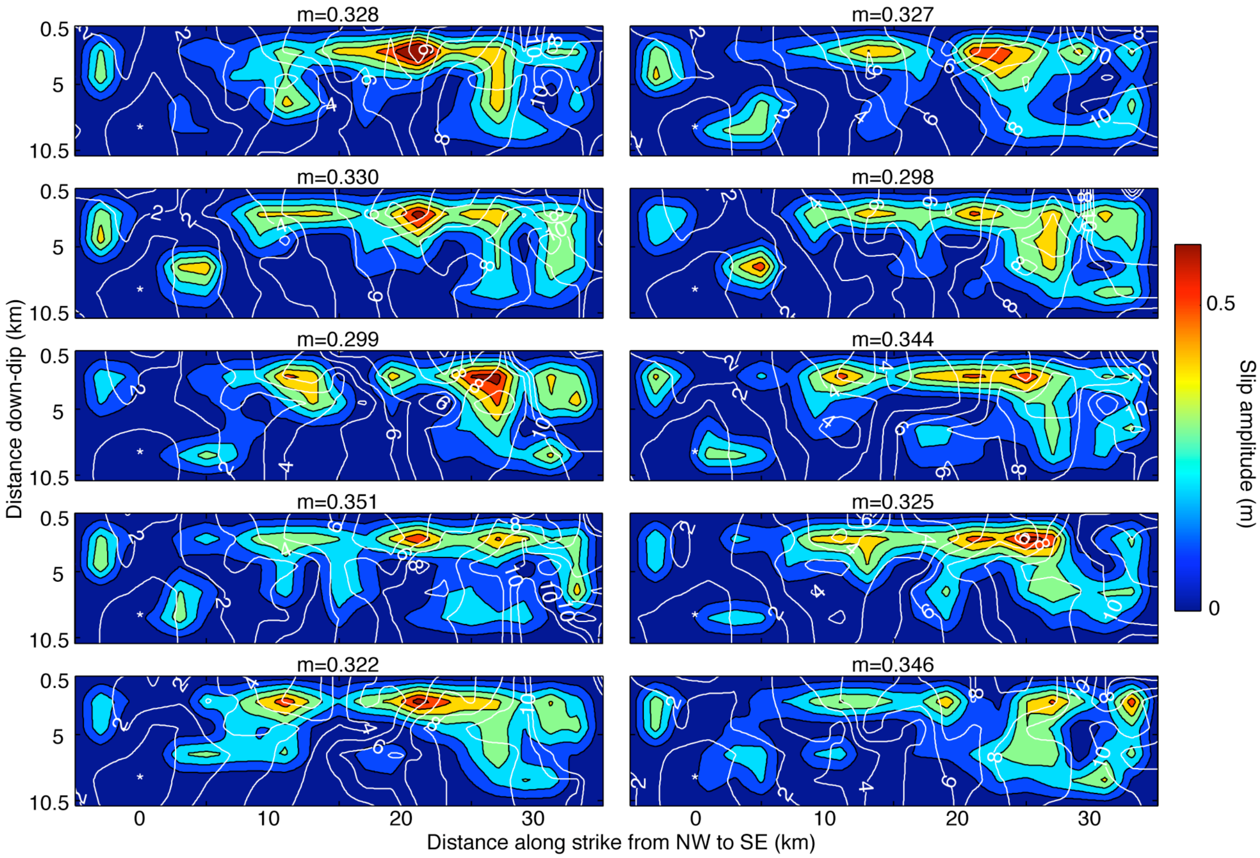

Figure fs01 (fs01.tif)

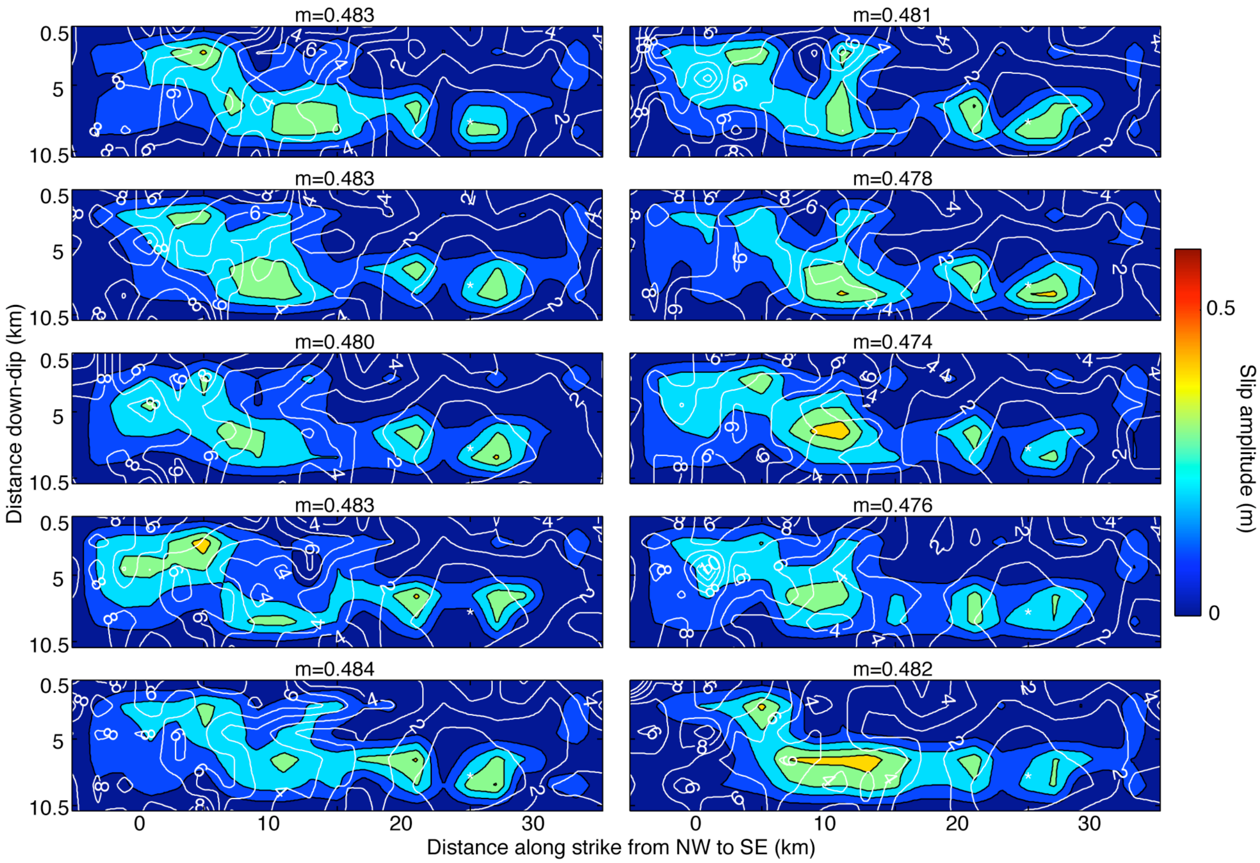

Figure fs02 (fs02.tif)